Joint iterative migration of electric and magnetic field data

Michael S. Zhdanov and Takumi Ueda, University of Utah

SUMMARY

Marine controlled-source electromagnetic (MCSEM) surveys become widely used in off-shore petroleum exploration. However, the interpretation of the MCSEM data is a very challenging problem because of the enormous amount of computations required in the case of the multi-transmitter and multi-receiver data acquisition systems used in these surveys. In this paper we demonstrate that this problem can be solved using the method of electromagnetic migration. We extend the basic principles of electric field migration to the case of joint electric and magnetic field interpretation. The joint migration field is produced by back propagation within the conductive sea-bottom sediments of all electric and magnetic signals recorded in the receivers. We demonstrate that the joint migration of the EM field data provides a better quality image of a sea-bottom resistive structure (e.g., a hydrocarbon reservoir) than the results of individual migration for the different (electric or magnetic) field components.

INTRODUCTION

In the paper presented at the SEG 2006 annual meeting, Zhdanov et al. (2006) introduced a new approach to the interpretation of the marine controlled-source electromagnetic (MCSEM) data, based on the ideas of electromagnetic holography and/or migration (Zhdanov, 1981; Zhdanov and Frenkel, 1983; Zhdanov et al., 1996; Zhdanov, 2001; Zhdanov, 2002; Tompkins, 2004; Mittet et al., 2005; Wan and Zhdanov, 2005). The physical principles of EM holography parallel those underlying optical holography and seismic migration. The recorded amplitudes and phases of an EM field scattered by the object form a broadband EM hologram. As in optical and radiowave holography, we can reconstruct the volume image of the object by "illuminating" the broadband EM hologram by the reference signal.

In the current paper, we extend the method of electromagnetic migration to a joint interpretation of the electric and magnetic components of the MCSEM data. The main goal of this paper is to demonstrate that the joint migration of the electric and magnetic fields can increase the resolution of the migration imaging.

APPLICATION OF ELECTROMAGNETIC MIGRATION TO MCSEM DATA INTERPRETATION

We consider a typical MCSEM survey consisting of a set of electric and magnetic field receivers located at the sea bottom, and an electric bipole transmitter moving at some elevation above the sea bottom, as shown in Figure 1. We assume that electrical conductivity in the model can be represented as the sum of a background conductivity $\sigma = \sigma_b$ and an anomalous conductivity $\Delta\sigma$ distributed within some local inhomogeneity D associated with the location of a petroleum reservoir. The receivers are located at the points with radius-vector $\mathbf{r}_j$ $(j = 1,2,3,...,J)$ in some Cartesian coordinate system. Every receiver R_j records the electric and magnetic field components of a field generated by an electric bipole transmitter moving above the receivers.

ELECTROMAGNETIC IMAGING USING JOINT MIGRATION OF ELECTRIC AND MAGNETIC FIELDS

The principles of EM holography/migration imaging are very similar to those of optical holography (Zhdanov, 2001). They can be summarized as follows.

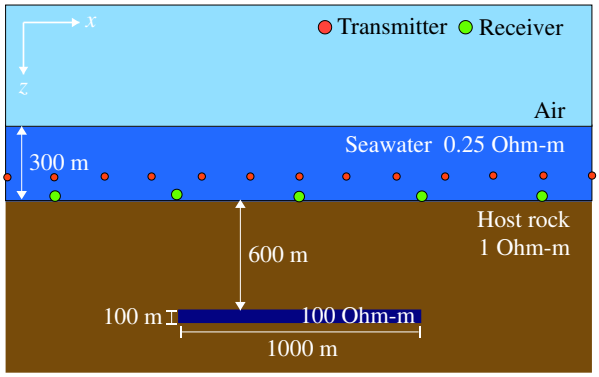

Figure 1: Sketch of the MCSEM survey and model design.

1) We "illuminate" the background media by a reciprocal electric dipole (in the case of electric observations) located in the actual receivers' positions to generate the "electric mode" background EM field $\left\{\widetilde{\mathbf{E}}^{bE},\widetilde{\mathbf{H}}^{bE}\right\}$. Alternatively, we "illuminate" the background media by a reciprocal magnetic dipole (in the case of the magnetic field observations) located in the actual receivers' positions to generate the "magnetic mode" background EM field $\left\{\widetilde{\mathbf{E}}^{bH},\widetilde{\mathbf{H}}^{bH}\right\}$.

2) We "illuminate" the background media by the artificial transmitters located in the positions of the true transmitters and represented by equivalent (fictitious) electric current dipoles. In the case of electric observations, the current moments are determined by the complex conjugate anomalous electric field observed in the true receiver for the given transmitter position. The electromagnetic field produced by this system of artificial electric dipoles generates the "electric mode" migration (backscattering) anomalous field $\left\{\widetilde{\mathbf{E}}^{mE},\widetilde{\mathbf{H}}^{mE}\right\}$. In the case of magnetic observations, the current moments are determined by the complex conjugate anomalous electric field multiplied by the factor $(-i\omega\mu)$. The electromagnetic field produced by this system of artificial transmitters generates the "magnetic mode" migration (backscattering) anomalous field $\left\{\widetilde{\mathbf{E}}^{mH},\widetilde{\mathbf{H}}^{mH}\right\}$.

3) In the case of electric field observations, the geoelectrical image of the sea-bottom inhomogeneities, $\mathbf{I}_0^E$, is formed by summation of the cross-power spectrum of the "electric mode" background and migration fields:

$$\mathbf{I}_0^E = \mathrm{Re}\sum\nolimits_{\omega_n}\left(\widetilde{\mathbf{E}}^{bE}\cdot\widetilde{\mathbf{E}}^{mE}\right), \tag{1}$$

where summation is done over all frequencies ω_n of the recorded fields.

4) In the case of magnetic field observations, the geoelectrical image of the sea-bottom inhomogeneities, $\mathbf{I}_0^H$ is formed by calculating the cross-power spectrum of the "magnetic mode" background and migration fields:

$$\mathbf{I}_0^H = \mathrm{Re}\sum\nolimits_{\omega_n}\left(\widetilde{\mathbf{E}}^{bH}\cdot\widetilde{\mathbf{E}}^{mH}\right). \tag{2}$$

5) In the case of joint migration of the electric and magnetic observed data, the geoelectrical image of the sea-bottom inhomogeneities, $\mathbf{I}_0^{EH}$,

is formed by summation of the "electric mode" and "magnetic mode" images:

$$\mathbf{I}_0^{EH} = \mathrm{Re}\sum\nolimits_{\omega_n}\left[\left(\widetilde{\mathbf{E}}^{bE}\cdot\widetilde{\mathbf{E}}^{mE}\right)+\left(\widetilde{\mathbf{E}}^{bH}\cdot\widetilde{\mathbf{E}}^{mH}\right)\right]. \qquad (3)$$

Note that, in the case of multi-receiver observations, the final image is produced by summation of all migration images generated for each receiver.

One can produce a better quality migration image by repeating the migration process iteratively. We begin with the migration of the observed data and migration conductivity analysis using the migration transformation and imaging conditions outlined above. In order to check the accuracy of our migration imaging, we apply the forward modeling and compute a residual between the observed and predicted data for the given conductivity model. If the residual is smaller than the prescribed accuracy level, we use the migration image as a final geoelectrical model. In the case where the residual is not small enough, we migrate the residual field and produce the corrections, $\delta\sigma_1$, to the original conductivity model using the same conductivity analysis, which we have applied to the original migration.

The iterative migration is terminated when the residual field becomes smaller than the required accuracy level of the data fitting. The mathematical details of the iterative migration algorithm are outlined in Zhdanov et al. (2006). It was demonstrated in that paper that the iterative migration, as well as iterative inversion, could be implemented using the smooth or focusing regularization. Particularly, images with sharp boundaries can be recovered using the minimum support (MS) or minimum gradient support (MGS) stabilizing functionals. This technique is implemented in our algorithm of the joint focusing migration of electric and magnetic field data.

Note that every iteration of the migration algorithm requires two forward modeling computations: one to compute the migration field, and another one for computing the predicted data in the receivers. In order to speed up the computations, we have implemented in our migration code a fast forward modeling method based on the multi-grid quasi-linear (MGQL) approximation, developed by Ueda and Zhdanov (2006). The multi-grid approach speeds up the computations significantly, while preserving the required accuracy of migration and forward modeling.

NUMERICAL STUDY OF THE JOINT ITERATIVE MIGRATION OF ELECTRIC AND MAGNETIC FIELDS

The joint iterative migration algorithm introduced in this paper was tested on several models of MCSEM surveys. In this abstract, we will present the results of this numerical study.

The MCSEM survey consists of two parallel transmitter-receiver profiles in the x direction. Each line consists of five sea-bottom receivers and an electric dipole transmitter moving along a line passing directly above the receivers at an elevation 50 m above the seafloor. In order to reduce the calculation cost, we assume that the transmitter generates a frequency domain EM field every 500 m along the towing line, which is extended from -4000 m to 4000 m. A total of ten seafloor electric receivers are located 5 m above the sea bottom along the x coordinates from $x = -2000$ to $x = 2000$ m with 1000 m spacing at $y = -500$ m and $+500$ m. The separation between receivers is 1000 m. The background layered geoelectrical model consists of a sea-water layer with a thickness of 300 m, a resistivity of 0.25 Ohm-m, and homogeneous sea-bottom sediments with a resistivity of 1 Ohm-m. There is an L-shaped reservoir located in the seafloor sediments at a depth of 900 m below the sea level with a resistivity of 100 Ohm-m, a thickness of 100 m, and a horizontal size of 2000 m by 2000 m. A 3D sketch of the true

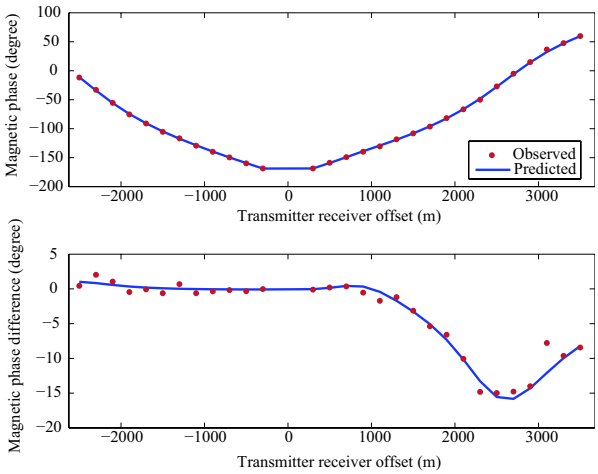

Figure 2: The top panel shows phase versus offset (PVO) plots of the total magnetic field, while the bottom panel present the PVO plot of the phase difference between the observed and background magnetic field. The observed data contaminated by the noise are shown by the red dots. The blue solid line corresponds to the data predicted for the migration resistivity model.

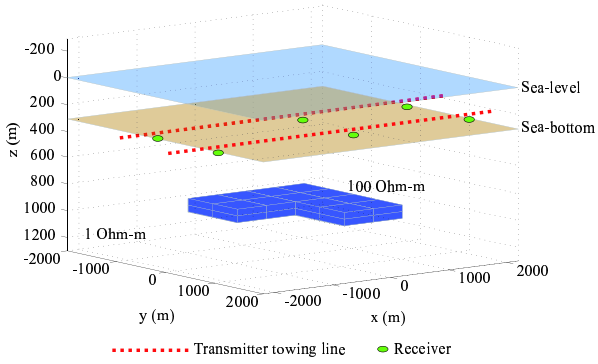

Figure 3: A 3D sketch of Model 2. The dashed lines denote transmitter towing profiles and the dots show the location of a sea-bottom receiver. The host rock has 1 Ohm-m resistivity, while the resistivity of the L-shaped reservoir is 100 Ohm-m.

resistivity model and transmitter-receiver locations is shown in Figure 3.

The transmitter generates an EM field at the frequencies of 0.125 and 0.25 Hz. The receivers measure the in-line component of the electric fields, E_x, and the cross-line component of the magnetic fields, H_y, simultaneously.

Note that we have contaminated the synthetic observed data with random Gaussian noise. The noise level increases linearly from 1% at zero offset up to 5% at 4,000 m offset to simulate the typical noise behavior in the field MCSEM data.

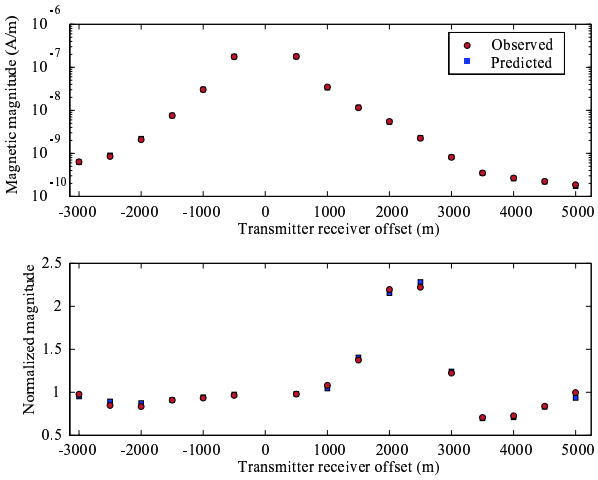

Figure 4: The top panel shows magnitude versus offset (MVO) plots of the total electric field, while the bottom panel presents an MVO plot of the same field normalized by the absolute values of the background electric fields. The observed data contaminated by noise are shown by the dots. The solid line corresponds to the data predicted for the migration resistivity model.

We apply the joint 3D inversion to the electric and magnetic data. Figure 6 shows the convergence plots for the same joint iterative migration process. The normalized parametric functional and the normalized residual reach 4% and 3% respectively at iteration #20. The corresponding migration image is shown in Figure 7 as the X-Y plan view at a depth of $z = 975$ m and in Figure 8 as 3D rendering of the true body and inversion result with a cut-off at 20 Ohm-m. We have also plotted in Figures 4 and 5 the predicted data computed for the migration model shown in Figure 8.

One can see that the L-shaped and depth of the reservoir are recovered extremely well in this image obtained by migration of the noisy EM data.

For comparison, Figure 9 presents the true model (a) and the imaging results obtained by migration of (b) two lines of electric and magnetic field data; (c) two lines of electric field data only; (d) two lines of magnetic field data only; (e) one line ($y = -500$ m) of joint electric and magnetic field data; (f) one line ($y = +500$ m) of electric and magnetic data.

We can see that some of these plots produce the distorted migration images of the L-shape reservoir. The joint migration of the two-line EM data generates the better quality image.

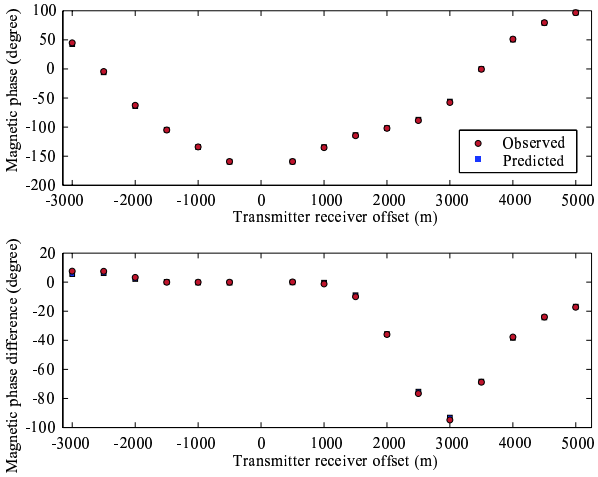

Figure 5: The top panel shows phase versus offset (PVO) plots of the total magnetic field, while the bottom panel presents a PVO plot of the phase difference between the observed and background magnetic fields. The observed data contaminated by noise are shown by the dots. The solid line corresponds to the data predicted for the migration resistivity model.

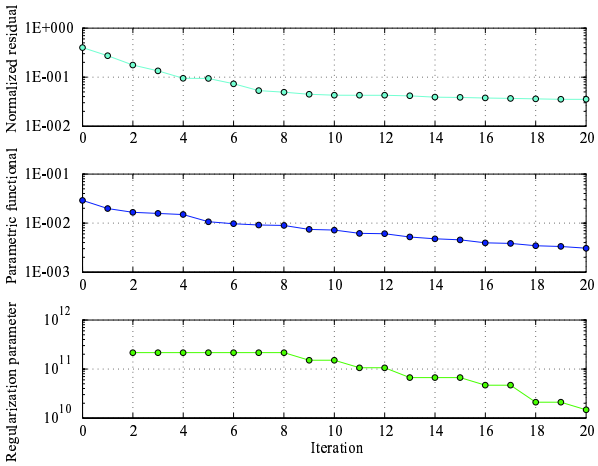

Figure 6: Convergence plots of the normalized residual (top panel) and parametric functional (middle panel) for joint iterative migration of the electric and magnetic fields for model 2. The bottom panel shows the behavior of the regularization parameter during the iterative migration.

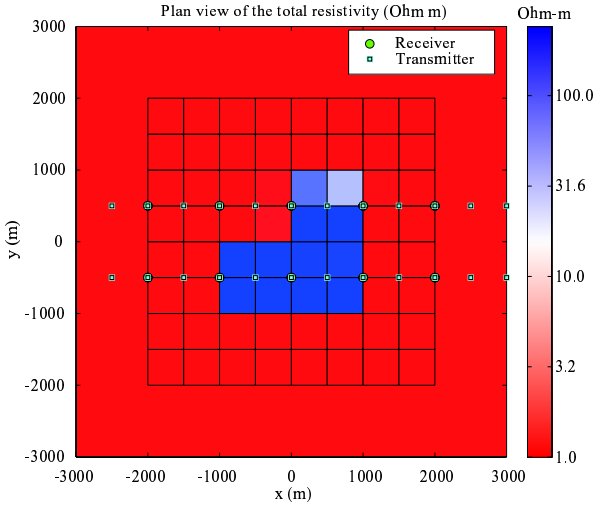

Figure 7: D X-Y plan view images of the final joint iterative migration result for Model 2 obtained by 3D migration of EM fields.

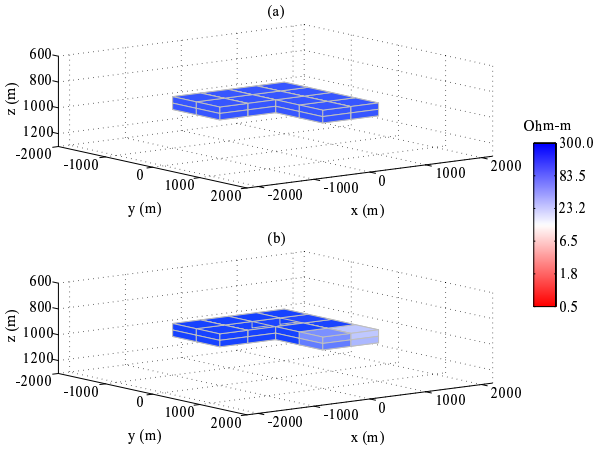

Figure 8: 3D images of (a) the true model and (b) the final joint iterative migration result for Model 2 obtained by 3D migration of EM fields.

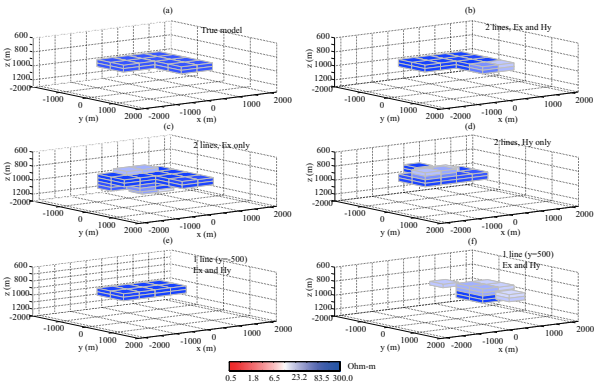

Figure 9: A 3D rendering of (a) true model and iterative migration results obtained by (b) two lines electric and magnetic data, (c) two lines electric field only, (d) two lines magnetic field data, (e) one line ($y = -500$ m) electric and magnetic data, and (f) one line ($y = +500$ m) electric and magnetic data.

CONCLUSION

The basic principles of electric field migration in application to MCSEM data interpretation are extended to the case of joint electric and magnetic field interpretation. The joint migration field is produced by a combination of all electric dipole transmitters operating simultaneously according to the recorded electric and magnetic signals in the receivers. We demonstrate that the joint migration of the EM field data provides a better quality image of a sea-bottom resistive structure than the results of individual migration for the different (electric or magnetic field components.

Future research will be focused on investigation of 3D MCSEM surveys with more complex geometry and interpretation of practical MCSEM data collected over real geological targets.

ACKNOWLEDGEMENTS

The authors acknowledge the support of the University of Utah Consortium for Electromagnetic Modeling and Inversion (CEMI), which includes BAE Systems, Baker Atlas Logging Services, BGP China National Petroleum Corporation, BHP Billiton World Exploration Inc., British Petroleum, Centre for Integrated Petroleum Research, EMGS, ENI S.p.A., ExxonMobil Upstream Research Company, INCO Exploration, Information Systems Laboratories, MTEM, Newmont Mining Co., Norsk Hydro, OHM, Petrobras, Rio Tinto - Kennecott, Rocksource, Russian Research Center Kurchatov Institute, Schlumberger, Shell International Exploration and Production Inc., Statoil, Sumitomo Metal Mining Co., and Zonge Engineering and Research Organization.